Journal of Physics:
Condensed Matter

PAPER • **OPEN ACCESS**

Effect of aliovalent substitution on the local structure of $CaKFe_4As_4$ superconductor

To cite this article: G Tomassucci *et al* 2024 *J. Phys.: Condens. Matter* **36** 475702

OPEN ACCESS
IOP Publishing
Journal of Physics: Condensed Matter
J. Phys.: Condens. Matter **36** (2024) 475702 (11pp)
https://doi.org/10.1088/1361-648X/ad6f89

Effect of aliovalent substitution on the local structure of $CaKFe_4As_4$ superconductor

G Tomassucci[1], L Tortora[1], F Minati[1], M Russo[1], A Duchenko[2], F Varsano[3], A Masi[4], G Campi[5], L Simonelli[6], V Martin-Diaconesu[6], L Boeri[1], T Mizokawa[7] and N L Saini[1,*]

[1] Dipartimento di Fisica, Universita' di Roma 'La Sapienza' - P. Aldo Moro 2, Roma, 00185, Italy
[2] Department of Industrial, Electronic and Mechanical Engineering, Universita' degli Studi Roma Tre, 00146 Roma, Italy
[3] ENEA, C. R. Casaccia, 000123 Roma, Italy
[4] ENEA, C. R. Frascati, 00044 Frascati, Italy
[5] CNR—Istituto di Cristallografia, 00015 Roma, Italy
[6] ALBA Synchrotron Light Facility, Carrer de la Llum 2-26, 08290, Cerdanyola del Valles, Barcelona, Spain
[7] Department of Applied Physics, Waseda University, Shinjuku 169-8555, Tokyo, Japan

E-mail: naurang.saini@uniroma1.it

Received 7 May 2024, revised 15 July 2024
Accepted for publication 14 August 2024
Published 30 August 2024

Abstract

We have investigated the local structure of the iron-based $CaKFe_4As_4$ superconductor featuring distinct aliovalent substitutions at the Ca and K sites, that is $CaKFe_4As_4$, $CaK_{0.9}Sr_{0.1}Fe_4As_4$, $CaK_{0.9}Ba_{0.1}Fe_4As_4$ and $Ca_{0.9}Na_{0.1}K_{0.9}Ba_{0.1}Fe_4As_4$. Temperature-dependent Fe K-edge extended x-ray absorption fine structure (EXAFS) measurements are used to determine the near-neighbors bondlengths and their stiffness. The EXAFS analysis reveals that the Fe–As bondlength undergoes negligible changes by substitution, however, the Fe–Fe bondlength and the As height are affected by the Sr substitution. The superconducting transition temperatures of $CaK_{0.9}Sr_{0.1}Fe_4As_4$ and $CaK_{0.9}Ba_{0.1}Fe_4As_4$ are very similar even if the mean As heights are significantly different suggesting that the anion height may not be a unique parameter to describe the superconductivity in $CaKFe_4As_4$. The mean As heights show a peculiar temperature dependence characteristic of $CaKFe_4As_4$ system. Furthermore, the temperature-dependent mean square relative displacements reveal similar Fe–Fe bond stiffness in all samples, instead the Fe–As bond is substantially stiffer in case of $CaK_{0.9}Sr_{0.1}Fe_4As_4$. The local structure results are discussed in relation to the differing transport properties of aliovalent substituted 1144 superconductor.

Keywords: iron-based superconductors, chemical doping, local structure, bond characteristics, EXAFS

* Author to whom any correspondence should be addressed.

1. Introduction

Since the discovery of superconductivity in $LaFeAsO_{1-x}F_x$ with a critical temperature of ~26 K [1], iron-based superconductors (FeSCs) have attracted significant attention from the scientific community owing to their intriguing properties, arising from a complex interplay of lattice, charge, and magnetic degrees of freedom [2, 3]. In this sense, the discovery has not only helped to advance the fundamental science of superconductivity but has also paved the way to design new layered functional materials aimed at desired application oriented properties [4–6]. As such, this has played a vital role in growing numerous FeSC with diverse structures and physical characteristics [4, 7–9]. Notable FeSC pnictides families include the 1111 type structures [1] (such as *Re*FeAsO, where *Re* represents rare-earth elements), the 122 type structures [10] (for example, $AeFe_2As_2$, where *Ae* denotes alkaline earth as Ca, Sr or Ba), and the 1144 type hybrid structures [11] (such as $AeAFe_4As_4$, with *A* being an alkaline metal as Na or K). The electron-doped 1111 type structure exhibits the highest superconducting transition temperature (T_c) reaching ~55 K [12, 13].

Most FeSCs require chemical doping or external pressure to achieve superconductivity. However, some stoichiometric compounds such as LiFeAs and FeSe are superconducting without any external doping [14, 15]. The 1144-type FeSC, which shows superconductivity at T_c as high as 36 K without any external doping or pressure [11, 16] is another self-doped system. This stoichiometric 1144 system is one of the compounds of interest to explore superconducting mechanisms without any interference from possible external disorder. The 1144 system with a tetragonal structure (see figure 1 showing the structure drawn by Vesta [17]) is a hybrid system with an ordered stacking of two different 122 structures [11], namely $AeFe_2As_2$ and AFe_2As_2. The stability of the 1144 structure depends on the size difference between the Alkaline earth (*Ae*) and Alkaline metal (*A*), causing the As layer in FeAs to be inequivalent in each substructure due to the alternate arrangement of *Ae* and *A* layers [18–20]. The most known compound among stable 1144 structures is $CaKFe_4As_4$, characterized by large hole doping [21]. Various experimental studies on thermodynamic and transport properties [22], angle-resolved photoemission spectroscopy (ARPES) [21, 23], nuclear magnetic resonance (NMR) [24], pressure effects [25] along with theoretical calculations [26], have been conducted on $CaKFe_4As_4$ to elucidate its diverse physical properties. Notably, two consecutive half-collapsed tetragonal transitions are found to occur in the 1144 structure under external pressure; one at ~4 GPa and the other at ~16 GPa while T_c decreases [27, 28]. Furthermore, Dirac surface states and Majorana zero modes have been identified in $CaKFe_4As_4$ for the first time in an FeSC [29]. On the application front, recent studies have discovered exceptional vortex pinning properties in $CaKFe_4As_4$ resulting from the inherent defect structure [30, 31], that gives rise to high value of the critical current density $\left(J_c \sim 10^8 \frac{A}{cm^2}\right)$, highest

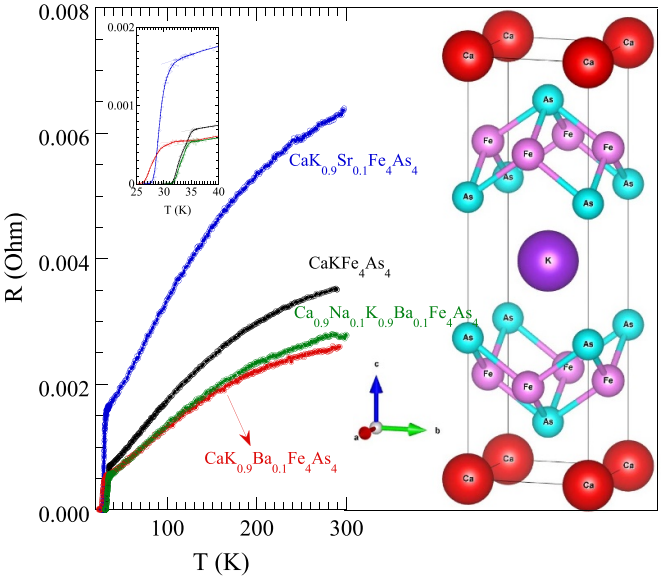

Figure 1. Resistance versus temperature curves of $CaKFe_4As_4$ with aliovalent substitutions. The residual resistance ratio (RRR), defined as R_{290K}/R_{36K}, is 5.0, 3.8, 4.6 and 5.0 for the pristine 1144, the Sr-substituted, the Ba substituted, and the charge compensated samples, respectively. A zoomover in the vicinity of the T_c is shown as inset. Crystal structure of $CaKFe_4As_4$ drawn using Vesta [17] from diffraction data at 300 K [11] is also shown.

reported for FeSC [32]. These properties suggest that 1144 family could also be a strong contender for high field applications of superconductivity.

A potential strategy for the physical properties optimization for practical applications could be a controlled increase in the configurational entropy of the 1144 system through elemental substitution [33, 34, 36–39]. For instance, Fe site substitutions have been found to effectively boost the critical current density [38, 39]. Nevertheless, it is important to note that any success through this approach comes at a cost, resulting in a significant reduction in the critical temperature, even with small quantity substitution. More recently, aliovalent substitutions of Ca or K have been exploited to manipulate physical properties of $CaKFe_4As_4$ [33–37]. Since the substitutions at the Ca or K in the stoichiometric compound are found to affect the superconducting properties as well as the structure stability, it is of key importance to investigate the local structure of the electronically active Fe–As network considering the fact that FeSCs are characterized by large electroelastic and magnetoelastic properties [2, 3].

In this work, we have studied the local structure of $CaKFe_4As_4$ for different aliovalent substitutions at Ca and K by extended x-ray absorption fine structure (EXAFS), a site selective experimental probe [40, 41]. In particular, the pristine $CaKFe_4As_4$, Sr substituted $CaK_{0.9}Sr_{0.1}Fe_4As_4$ and Ba substituted $CaK_{0.9}Ba_{0.1}Fe_4As_4$ in which electrons are formally introduced to the FeAs layer by the substitutions, and charge compensated $Ca_{0.9}Na_{0.1}K_{0.9}Ba_{0.1}Fe_4As_4$ have been

analyzed for their local structure. Temperature-dependent Fe K-edge EXAFS measurements have been used to investigate bond characteristics and local displacements around iron. The EXAFS data reveal that the Fe–As bondlengths are hardly affected by the substitutions, while the Fe–Fe bonds along the *a*-axis of the unit cell present notable changes and hence the anion height. Incidentally, the Sr substituted system shows stiffer bonds, likely to be due to possible texturing in this system. The results are discussed in relation with the coordinated role of charge density and size effect in driving the transport properties of $CaKFe_4As_4$ FeSCs.

2. Experimental details

Temperature-dependent Fe K-edge (7.11 keV) x-ray absorption measurements were carried-out on polycrystalline samples of pristine $CaKFe_4As_4$, Sr-substituted $CaK_{0.9}Sr_{0.1}Fe_4As_4$, Ba-substituted $CaK_{0.9}Ba_{0.1}Fe_4As_4$, and charge compensated $Ca_{0.9}Na_{0.1}K_{0.9}Ba_{0.1}Fe_4As_4$ with Na- and Ba-substitution. These samples were prepared following the detailed method outlined previously [36]. The homogeneity of the powders is ensured by the high-energy ball milling treatment. The low temperature synthesis route allows to minimize volatile elements loss, and the nominal compositions do not show any significant deviations from the actual content [34–37] apart from the unavoidable contamination of oxygen of the starting reactants. Figure 1 displays the resistance versus temperature curves for the samples, showing T_c (onset) of ~35 K, 32 K, 31 K and 34 K respectively. The residual resistance ratio (RRR), estimated as R_{290K}/R_{36K} are found to be 5.0, 3.8, 4.6 and 5.0 for the pristine 1144, the Sr-substituted, the Ba substituted, and the charge compensated samples, respectively. The details of the samples characterization and their structural, electrical, and magnetic transport can be found elsewhere [33, 36, 37].

The x-ray absorption measurements in the transmission mode took place at the CLAESS beamline of the 3 GeV ALBA synchrotron radiation facility in Cerdanyola del Valles (Barcelona) [42]. The CLAESS beamline is a multipole wiggler beamline consisting of 12 periods with a total length of 1 m. A double crystal Si(111) monochromator coupled with a rhodium-coated focusing mirrors to eliminate higher harmonics, was a part of the experimental setup. The measurement setup featured three ionization chambers: two for capturing the incident intensity (I_0) and transmitted intensity (I_t) of x-rays, and one for monitoring the transmission across an iron foil used as reference. The samples, sealed in an evacuated quartz ampule, were opened in a glove box and placed in a continuous flow liquid helium cryostat. The measurement temperatures were selected to be in the range from 20 K to room temperature with a control within ±1 K during the measurements. At least four absorption scans were acquired at each temperature to ensure spectral reproducibility and high signal-to-noise ratio. The EXAFS oscillations were extracted from the energy dependent x-ray absorption spectra using the standard procedure in which polynomial spline fit of the pre-edge subtracted absorption spectrum is used [40, 41].

3. Results and discussions

We have measured the Fe K-edge x-ray absorption spectra at several temperatures on the four samples, mounted on the same sample holder that was placed in the same experimental conditions. Figure 2 shows the EXAFS oscillations at several temperatures for the pristine $CaKFe_4As_4$, Sr-substituted $CaK_{0.9}Sr_{0.1}Fe_4As_4$, Ba-substituted $CaK_{0.9}Ba_{0.1}Fe_4As_4$ and charge compensated $Ca_{0.9}Na_{0.1}K_{0.9}Ba_{0.1}Fe_4As_4$ samples, plotted as a function of the wavevector *k*. The EXAFS oscillations can be seen up to $k \sim 15\,\text{Å}^{-1}$ for all samples with a clear evolution in temperature. The EXAFS oscillations are due to the photoelectron wave excited from the Fe atom, interfering with the backscattered wave from the surrounding atoms in the 1144 structure. Therefore, the EXAFS oscillations carry information about the partial pair distribution function around the selected photoabsorbing Fe atom. The partial pair distribution can be seen in the Fourier transforms (FTs) of the EXAFS oscillations displayed in figure 3. The k-range for the FTs is 3-15 Å^{-1} and a Gaussian window has been applied. In the average crystal structure of $CaKFe_4As_4$ (figure 1) there are four As near neighbors of Fe at ~2.4 Å (i.e. Fe-As bondlengths) and the four Fe next near neighbors at ~2.7 Å (Fe-Fe bondlengths) and the peak at ~2.2 Å contains mixed contributions of these neighbors around the photoabsorbing Fe in FTs. Weaker peak features beyond ~ 3 Å are due to farther neighbors (longer distances) and due to multiple scattering contributions. In particular, farther atoms from Fe are expected to be Ca (Na) atoms at ~3.17 Å, K (Sr Ba) atoms at ~3.47 Å and the next Fe atoms at ~3.87 Å comprising peak structures in the R-interval of 2.7–4 Å. There are some apparent changes including those in the bondlengths (indicated by the vertical dashed guides).

The local structure parameters can be obtained by EXAFS model fits. Since the focus in this work is the $FeAs_4$ network, the model fits are limited to the nearest neighbors As and Fe atomic shells for which a single scattering approximation remains valid while farther atoms are not considered. The standard EXAFS equation based on a single scattering approximation is given by [40, 41]:

$$\chi(k) = \sum_i \frac{N_i S_0^2}{kR_i^2} |f_i(k,R_i)| e^{-\frac{2R_i}{\lambda}} e^{-2k^2\sigma_i^2} \sin\left(2kR_i + \delta_i(k)\right). \tag{1}$$

Here, N_i represents the number of *i*th neighboring atoms at a distance R_i from the photoabsorbing atom while δ_i is the phase shift and $f_i(k,R_i)$ is the backscattering amplitude. The EXAFS amplitude is also affected by the photoelectron mean free path λ and the parameter σ_i^2 describing the correlated Debye–Waller factor (DWF) that measures the mean square relative

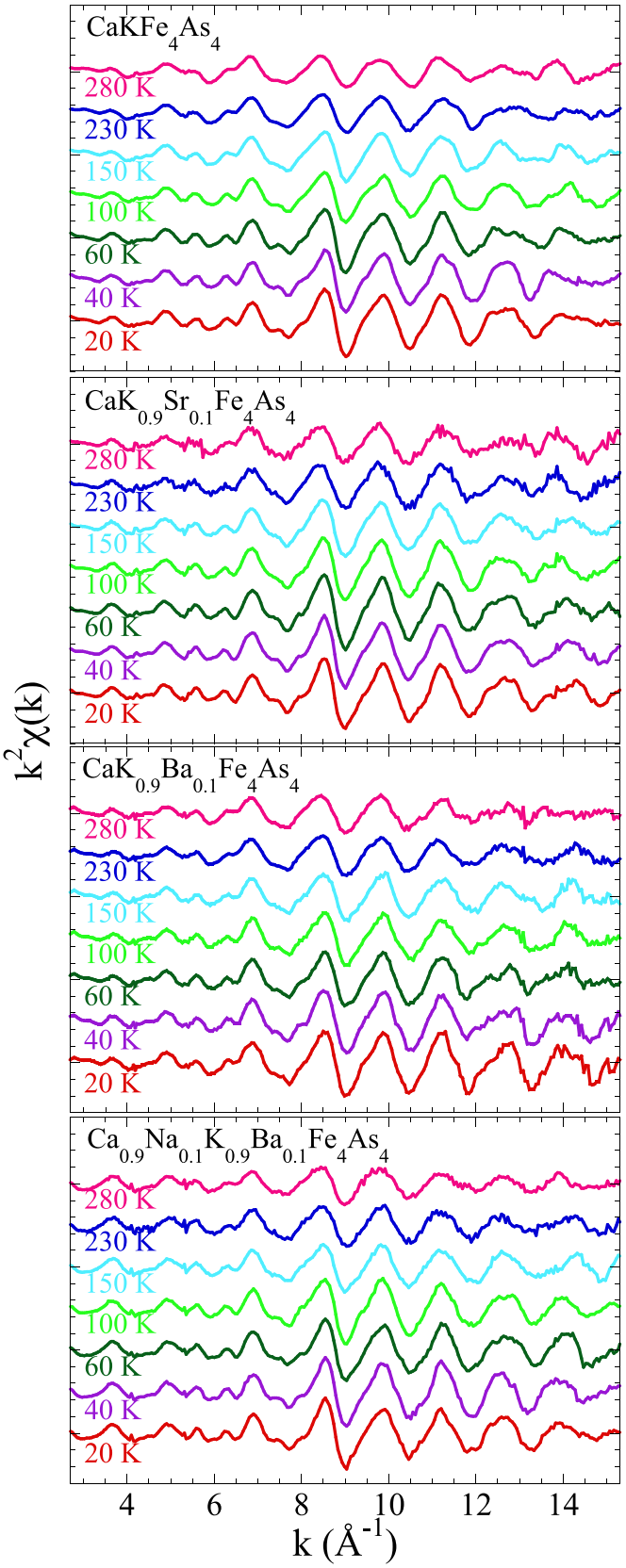

Figure 2. Temperature evolution of Fe K-edge EXAFS oscillations (weighted by k^2) of $CaKFe_4As_4$, $CaK_{0.9}Sr_{0.1}Fe_4As_4$, $CaK_{0.9}Ba_{0.1}Fe_4As_4$, $Ca_{0.9}Na_{0.1}K_{0.9}Ba_{0.1}Fe_4As_4$. Measurements were made in transmission mode in a temperature range between 20 K and 280 K. The EXAFS spectra have been shifted vertically for better visualization.

displacements (MSRDs) of the pair of atoms (photoabsorber-backscatter pairs). The scale factor (S_0^2), also called passive electrons reduction factor, is due to many-body effects associated to the losses (excitations as plasmons, electron–hole pairs, etc) occurring during the photoelectron propagation in the material and the intrinsic losses due to shake-up and shake-off excitations created by the core-hole in the absorption process [40, 41].

The starting structural model used for the EXAFS analysis is provided by the average crystal structure [11]. We should recall that $CaKFe_4As_4$ is characterized by two inequivalent positions of As atoms and hence two Fe–As distances are separated by ~0.02 Å. However, the separation could not be resolved with the experimental resolution ($\Delta R = \frac{\pi}{2k_{max}} \sim 0.1$ Å, with $k_{max} = 15$ Å^{-1}) in the present experiment, and hence for simplicity we have used an average Fe–As distance and obtained satisfactory model fits. The EXCURVE code [43] was used to calculate the backscattering amplitudes and phase shift functions considering the Muffin-Tin approximation. The same code was later used to perform the model fits, fixing S_0^2 and E_0 (photoelectron energy zero), same for all samples, after a number of trials and leaving the atomic positions R_i and related σ_i^2 as the free parameters. The number of independent data points, $N_{ind} \sim \frac{2\Delta k \Delta R}{\pi}$, was about 14 for the fit intervals in the k space $\Delta k = 12$ Å^{-1} (3.0–15.0 Å^{-1}) and in R space $\Delta R = 1.8$ Å (1.2–3.0 Å). The real-space model fits were also carried out by the WINXAS package [44] in which the scattering amplitudes and phase shifts were calculated by FEFF code [45], obtaining same results for the two shells. The two-shells model fits in the real-space are shown together with the corresponding experimental FTs (weighted by k^2) in figure 3. The quality of the fits is judged by the R-factor describing the fractional misfit defined as:

$$R = \frac{\sum_{i=1}^{N} |\chi_{th}(r_i) - \chi_{exp}(r_i)|^2}{\sum_{i=1}^{N} |\chi_{exp}(r_i)|^2}. \quad (2)$$

Here, the number of data points is given by N, while experimental and theoretical EXAFS signals are $\chi_{exp}(r_i)$ and $\chi_{th}(r_i)$. For the model fits in the k-space the R–factors were in the range of 30–40 (depending on the temperature), indicating satisfactory EXAFS fits of unfiltered EXAFS. The uncertainties in the measured parameters were determined by analysis of multiple EXAFS scans at each temperature. The contribution to the uncertainties due to correlations between different parameters was determined by creating the correlation maps [46].

The temperature dependence of the average local Fe–As bondlengths are shown in figure 4. The Fe–As bondlength changes almost linearly with temperature in all samples. In the pristine $CaKFe_4As_4$ sample, the mean Fe-As distance at low temperature is found to be ~2.385 Å, showing a weak temperature dependence (linear thermal expansion coefficient $\alpha_{Fe-As} \sim 7.7 \times 10^{-6}$ K^{-1}), similar to the one reported in a previous study [47]. The local Fe–As bondlength, measured on the powder sample in this work, is slightly longer (~0.01 Å) than the one reported earlier by polarized EXAFS on a single

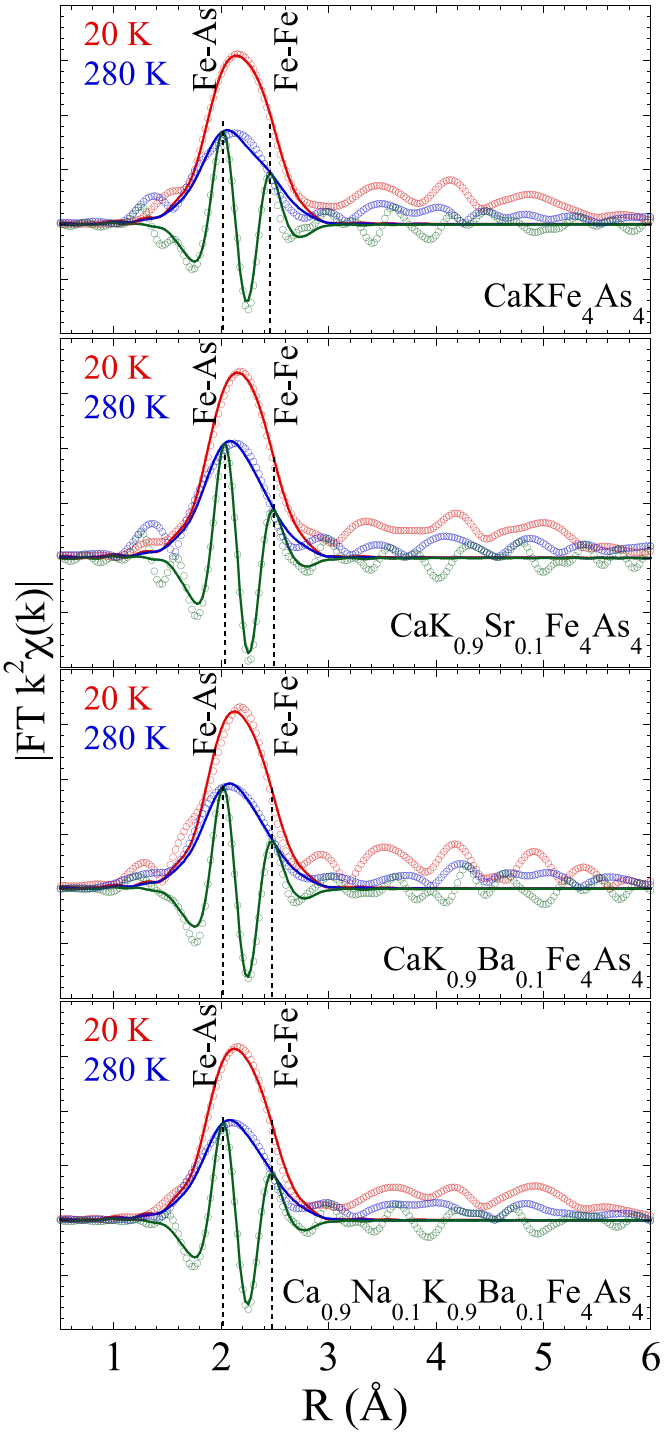

Figure 3. Fourier transform magnitudes of the EXAFS oscillations of $CaKFe_4As_4$, $CaK_{0.9}Sr_{0.1}Fe_4As_4$, $CaK_{0.9}Ba_{0.1}Fe_4As_4$, and $Ca_{0.9}Na_{0.1}K_{0.9}Ba_{0.1}Fe_4As_4$ (weighted by k^2) at 20 K and 280 K (open circles) along with the two-shells model fits (solid lines). The real part of the FT at 280 K with the model fit is also included. The fit window in real space is 1.2–3.0 Å.

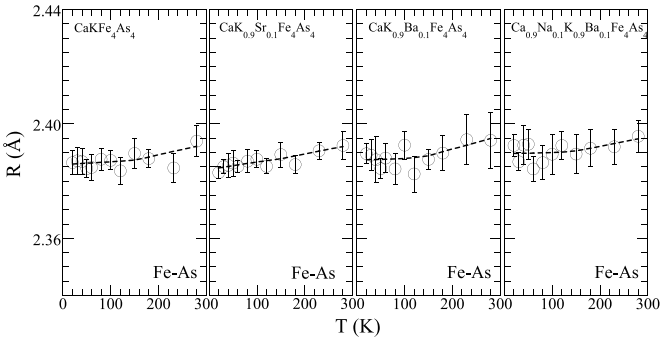

Figure 4. Temperature dependence of the local Fe–As bondlengths determined by the Fe K-edge EXAFS analysis for $CaKFe_4As_4$, $CaK_{0.9}Sr_{0.1}Fe_4As_4$, $CaK_{0.9}Ba_{0.1}Fe_4As_4$, and $Ca_{0.9}Na_{0.1}K_{0.9}Ba_{0.1}Fe_4As_4$. The dashed line is a smooth curve that also underlines the thermal expansion of Fe–As bonds.

crystal of $CaKFe_4As_4$ [47], likely to be due to intrinsic anisotropy of the atomic vibrations in the system. The Fe-As bondlength shows negligible change by the partial substitution of Sr (Alkaline earth) in place of K (Alkaline metal). Indeed, the Fe-As bond (~2.384 Å) as well as the linear thermal expansion coefficient ($\alpha_{Fe-As} \sim 1.1 \times 10^{-5}\,K^{-1}$) is similar to the one in the pristine $CaKFe_4As_4$. It should be recalled that the Sr^{2+} (1.32 Å) is much smaller than K^{1+} (1.52 Å) and hence a substantial chemical pressure due to the size difference can be expected. In addition, there is a partial removal of hole concentration in the FeAs layer. However, these factors seem to have limited effect on the covalent Fe–As bondlength itself. Similarly, the Ba (Alkaline earth) substitution in place of K has limited effect on the Fe-As bondlength (~2.387 Å) with the linear thermal expansion ($\alpha_{Fe-As} \sim 1.3 \times 10^{-5}\,K^{-1}$) being very similar. Also in this case, hole concentration in the FeAs layer should be reduced apart from the smaller size difference between the Ba^{2+} (1.49 Å) and the K^{1+} (1.52 Å). The simultaneous substitution of Na and Ba in place of Ca and K respectively is a charge compensation process considering that Na^{1+} (1.16 Å) is substituted for Ca^{2+} (1.14 Å) and Ba^{2+} for K^{1+} with the size difference being smaller than the earlier cases. Indeed, the Fe–As bondlength (~2.388 Å) shows negligible change as the others, and the linear thermal expansion coefficient ($\alpha_{Fe-As} \sim 6.7 \times 10^{-6}\,K^{-1}$) remains similar. Therefore, the strongest bondlength in the 1144 system is hardly affected by the substitutions.

Unlike the Fe–As, the Fe–Fe bondlengths shown in figure 5, seem more sensitive to the substitutions, appearing different for differently substituted samples. The mean Fe–Fe bondlength in $CaKFe_4As_4$ is ~2.719 Å, consistent with the previous EXAFS study on a single crystal sample [47]. Apparently, the Fe–Fe bondlength tends to change anomalously with temperature. The mean value of the Fe-Fe bondlength in $CaK_{0.9}Sr_{0.1}Fe_4As_4$ (~2.732 Å) is significantly longer than the one in $CaKFe_4As_4$. This shows that the nominal Sr substitution in place of K expands the in-plane Fe–Fe lattice keeping the Fe–As bondlength almost unaffected. This is consistent with the diffraction studies [37] showing expanded *a*-axis in the Sr substituted sample with respect to the pristine $CaKFe_4As_4$. Similar to $CaK_{0.9}Sr_{0.1}Fe_4As_4$, the Ba-substituted $CaK_{0.9}Ba_{0.1}Fe_4As_4$ also shows slight expansion of the in-plane lattice with the Fe–Fe distance being ~2.723 Å,

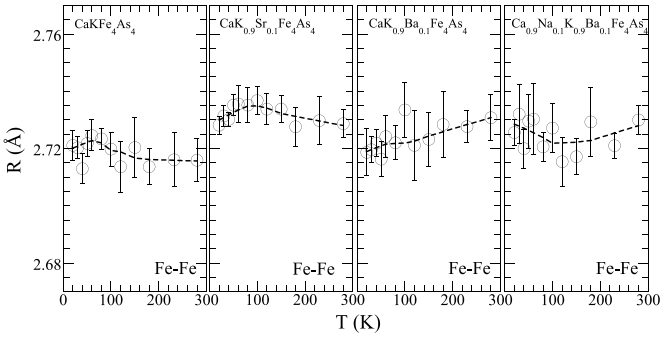

Figure 5. Temperature dependence of Fe–Fe bondlengths for $CaKFe_4As_4$, $CaK_{0.9}Sr_{0.1}Fe_4As_4$, $CaK_{0.9}Ba_{0.1}Fe_4As_4$, and $Ca_{0.9}Na_{0.1}K_{0.9}Ba_{0.1}Fe_4As_4$ as a function of temperature. The dashed line is a smooth curve to guide the eyes.

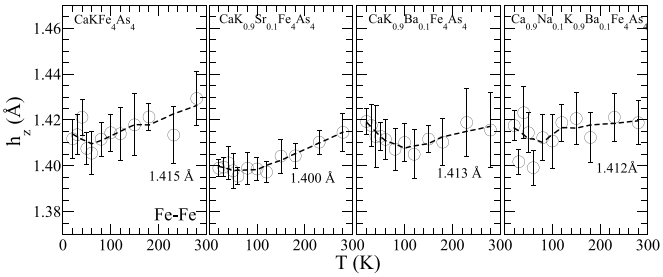

Figure 6. Temperature dependence of mean As height above the Fe plane obtained from least-square fitting of the Fe K-edge EXAFS oscillations for $CaKFe_4As_4$, $CaK_{0.9}Sr_{0.1}Fe_4As_4$, $CaK_{0.9}Ba_{0.1}Fe_4As_4$, and $Ca_{0.9}Na_{0.1}K_{0.9}Ba_{0.1}Fe_4As_4$. The dashed line is a smooth curve to guide the eyes.

slightly shorter than the one in $CaK_{0.9}Sr_{0.1}Fe_4As_4$, likely to be due to smaller size difference between Ba and K. Again, slightly longer Fe–Fe bondlength with respect to the pristine $CaKFe_4As_4$ is consistent with the diffraction results showing expansion of the *a*-axis in the Ba substituted sample [37]. Finally, in charge compensated $Ca_{0.9}Na_{0.1}K_{0.9}Ba_{0.1}Fe_4As_4$, the Fe–Fe distance is ~2.724 Å, similar to the Ba substituted sample but longer than the one in the pristine 1144 system. This is consistent with the smaller size difference, however, inconsistent with the diffraction studies showing *a*-axis of the system to be very similar to the one in $CaKFe_4As_4$. However, it is worth recalling that diffraction profiles for $Ca_{0.9}Na_{0.1}K_{0.9}Ba_{0.1}Fe_4As_4$ are much broader [37] and a detailed analysis of the diffraction data is desirable to obtain complete information on the lattice parameters in a crystallographically disordered system.

The As height above the Fe–Fe plane h_{As} in the $FeAs_4$ tetrahedron is commonly used to describe the correlation between the local structure and the superconductivity in FeSCs [48]. It is possible to determine h_z from a simple geometrical relationship assuming tetragonal symmetry, i.e.;

$$h_z = \sqrt{R^2_{\mathrm{Fe-As}} - \frac{1}{2}R^2_{\mathrm{Fe-Fe}}}. \tag{3}$$

The mean As anion heights (h_z), determined using the local Fe–As and Fe–Fe bondlengths, are shown in figure 6. Although small, the h_z shows a tendency of shrinkage with decreasing temperature before tending to elongate across ~100 K. This temperature behavior of the As height should be characteristic of $CaKFe_4As_4$ family as the same trend has been seen in the earlier work in which polarized EXAFS on a single crystal sample was used [47]. It is possible that the system goes through the half collapsed phase transition [27, 28] below ~100 K in which the local As–As bonding affects the h_z value. However, unlike the earlier study on $CaKFe_4As_4$ [47], we do not see any change below T_c within the experimental uncertainties.

The mean anion height in the pristine $CaKFe_4As_4$ is ~1.415 Å, consistent with the diffraction results, however, slightly longer than the one measured by EXAFS in single crystal sample [47]. The h_z in $CaK_{0.9}Sr_{0.1}Fe_4As_4$ is much shorter, being ~1.400 Å. Instead, the mean anion heights in $CaK_{0.9}Ba_{0.1}Fe_4As_4$ and in charge compensated $Ca_{0.9}Na_{0.1}K_{0.9}Ba_{0.1}Fe_4As_4$ (~1.413 Å and ~1.412 Å respectively) are very similar but tend to be shorter than the one in the pristine $CaKFe_4As_4$. Apparently, the empirical relationship [48] between the anion height and the T_c behavior is not applicable to the present systems. The pristine $CaKFe_4As_4$ with the anion height ~1.415 Å shows $T_c \sim 35$ K and should be located at the right side of the empirical relationship curve [48]. The $T_c \sim 32$ K is lower for $CaK_{0.9}Sr_{0.1}Fe_4As_4$ [33, 36] showing lower h_z. Similarly, the T_c of charge compensated $Ca_{0.9}Na_{0.1}K_{0.9}Ba_{0.1}Fe_4As_4$ with the anion height very similar to the pristine 1144 is slightly lower (~34 K) and, once more the reduced T_c of this system with respect to the pristine $CaKFe_4As_4$ cannot be described by the empirical relationship. Finally, $CaK_{0.9}Ba_{0.1}Fe_4As_4$ is characterized by lower T_c than the one for the pristine 1144 system while the anion height is almost similar (or slightly lower). Again, this is further indication that, within the same family of FeSCs, the anion height may not be the unique parameter and the local strain should have some optimum value as well as the charge density in the multi-component superconductors.

Further insight into the local disorder and bond character (i.e. orbital overlap) can be obtained from the σ_i^2 parameter, i.e. the MSRDs of the pair of atoms. The σ_i^2 is the sum of a temperature independent term σ_0^2, describing the configurational disorder, and a temperature dependent term, related to the bond character, i.e. $\sigma^2 = \sigma_0^2 + \sigma^2(T)$. The $\sigma^2(T)$ is well described by the correlated Einstein model equation [41, 49], i.e.;

$$\sigma^2(T) = \frac{\hbar^2}{2\mu k_B \Theta_E} \coth\left(\frac{\Theta_E}{2T}\right) \tag{4}$$

where μ is the reduced mass of the atomic pair, k_B is the Boltzmann's constant and Θ_E is the Einstein temperature, related with the frequency of the Einstein mode by $k_B\Theta_E = \hbar\omega_E$. The σ_i^2 parameter for the Fe–As and Fe–Fe pairs as a

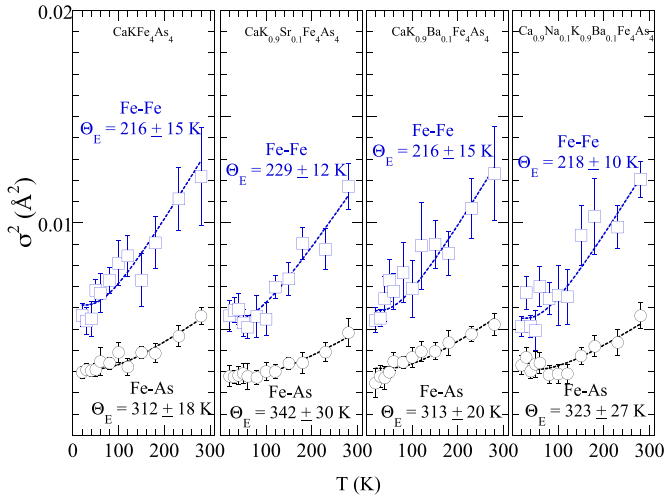

Figure 7. Mean square relative displacements (MSRD) of the Fe–As (circles) and Fe–Fe (squares) pairs as a function of temperature in $CaKFe_4As_4$, $CaK_{0.9}Sr_{0.1}Fe_4As_4$, $CaK_{0.9}Ba_{0.1}Fe_4As_4$, and $Ca_{0.9}Na_{0.1}K_{0.9}Ba_{0.1}Fe_4As_4$. The dashed lines represent the Einstein model fits on the experimental data.

function of temperature is shown in figure 7. The temperature behavior of the σ_i^2 is satisfactorily described by the correlated Einstein model equation (equation (4)) permitting us to determine the Einstein temperature for the atomic pairs, i.e. the bond stiffness $\kappa = \mu\omega_E^2$, as summarized in table 1.

The Einstein temperature of Fe–As bond is hardly affected by the Ba substitution at the K site. Indeed, the $\Theta_E \sim 312$ K for the pristine 1144 system, similar to the value reported in a previous study [47], does not differ from the one for the Ba substituted system ($\Theta_E \sim 313$ K). This indicates that the partial charge extraction (substitution of K^{1+} by Ba^{2+}) with small size difference has negligible effect on the Fe–As bond stiffness, i.e. Fe 3*d*-As 4*p* orbital overlap. Instead, we can see that the substitution of Sr leads to a substantial change in the Fe–As bond stiffness with the Θ_E being ∼342 K for this bond in $CaK_{0.9}Sr_{0.1}Fe_4As_4$. The only difference between the Ba and Sr is the size difference, and the Ba substitution hardly affects the Fe–As stiffness while the Sr substitution does. Therefore, the chemical pressure reduces the As height and increases the Fe 3*d*-As 4*p* orbitals hybridization. In the charge compensated $Ca_{0.9}Na_{0.1}K_{0.9}Ba_{0.1}Fe_4As_4$ system, the Fe–As bond is characterized by $\Theta_E \sim 323$ K. The substitution at the K site hardly affects the Fe–As bond rigidity while the substitution at the Ca site does, suggesting contrasting role of the Alkaline earths and Alkaline metals in defining the properties of the Fe–As bond network in 1144 superconductors.

X-ray absorption near edge structure (XANES) is a sensitive probe of the local geometry and the valence electronic states [40] and provides useful information on the orbitals hybridization. Figure 8 shows the Fe K-edge XANES of the four samples at $T = 20$ K. The spectra are normalized with respect to the atomic absorption, estimated via a linear fit far from the absorption edge jumps. The main spectral features are denoted as P, A_1, A_2, B and C. The spectral differences with respect to the pristine $CaKFe_4As_4$ are also shown reflecting the changing local geometry and the valence electronic states by the aliovalent substitution. The spectral differences are mainly in the region of the peaks P, A_1, A_2 with the maximum difference being ∼6%.

The Fe K-edge absorption process is mainly described by the Fe $1s \rightarrow 4p$ dipole transition in the continuum. In addition, a quadrupole transition in the unoccupied Fe 3*d* orbitals is possible that appears as a pre-peak P. The peak P also contains dipole contribution due to local distortions [50] mixing d and p-symmetry orbitals [51]. A zoom over the peak P for the four samples is compared in the inset of figure 8. The quadrupole $1s \rightarrow 3d$ transition is expected to be weak, however, due to the hybridization of the Fe 3*d* orbitals with the As 4*p* the peak P appears significantly intense in the FeSCs [51, 52]. On the other hand, the features A_1, A_2, B and C are due to transitions in the continuum and sensitive to the local geometry of the system.

The XANES differences clearly show that the local geometry is substantially affected by the aliovalent substitution. It appears that Sr substitution introduces largest change in the local geometry with A_1 and A_2 being most intense. The charge compensating Na and Ba substitutions and Ba substitution appear to have almost the same magnitude of local geometrical effect. On the other hand, peak P is most intense for the Sr substituted sample and least intense for the Ba substituted sample while remains unaltered for the charge compensated sample. This is a direct evidence of increased hybridization of the 3*d* and the As 4*p* orbitals, consistent with the conclusion drawn by EXAFS on the basis of measured As height.

Within the experimental uncertainties, the Fe-Fe bond character (i.e. the bond stiffness) remains the same for $CaKFe_4As_4$, $CaK_{0.9}Ba_{0.1}Fe_4As_4$, and $Ca_{0.9}Na_{0.1}K_{0.9}Ba_{0.1}Fe_4As_4$ samples with the Θ_E of this bond being ∼216 K, ∼216 K and ∼218 K respectively. However, the same bond tends to be stiffer in $CaK_{0.9}Sr_{0.1}Fe_4As_4$ with $\Theta_E \sim 229$ K. The Einstein temperatures for the Fe-Fe bond are consistent with the earlier studies on Fe-pnictides [53, 54] including the 1144 system [47]. Therefore, it can be safely stated that the small substitution in $CaKFe_4As_4$ has negligible effect on the Fe-Fe bond character. The local structure parameters are summarized in table 1.

Here, it is worth recalling that the stability of 1144 structure is primarily driven by the size effect and the charge density [11, 19, 20]. In charge compensated $Ca_{0.9}Na_{0.1}K_{0.9}Ba_{0.1}Fe_4As_4$, the transition temperature is not affected with respect to the pristine 1144 system indicating that hole concentration in the FeAs layer is likely be the primary factor for the superconductivity in the system within its stability range. In fact, the substitutions of Ba and Sr affect the hole concentration, and hence a substantial reduction in T_c from ∼35 K to ∼31 K should be understandable. However, it should be interesting to see how the size difference affects the transition temperature. This question is also relevant considering the fact that the T_c is hardly affected under small external pressure [27, 28]. On

Table 1. The local structure parameters of $CaKFe_4As_4$, $CaK_{0.9}Sr_{0.1}Fe_4As_4$, $CaK_{0.9}Ba_{0.1}Fe_4As_4$, and $Ca_{0.9}Na_{0.1}K_{0.9}Ba_{0.1}Fe_4As_4$ determined from the Fe K-edge EXAFS. The transition temperatures (T_c (onset)) are also included.

	$CaKFe_4As_4$ $T_c = 35$ K			$CaK_{0.9}Sr_{0.1}Fe_4As_4$ $T_c = 32$ K		
	Θ_E(K)	κ(eV Å^{-2})	σ_0^2(Å^2)	Θ_E(K)	κ(eV Å^{-2})	σ_0^2(Å^2)
Fe–As	312 ± 18	5.5(3)	0.0007(2)	342 ± 30	6.6(6)	0.0006(3)
Fe–Fe	216 ± 15	2.3(2)	0.0022(5)	229 ± 12	2.6(1)	0.0017(4)
	$CaK_{0.9}Ba_{0.1}Fe_4As_4$ $T_c = 31$ K			$Ca_{0.9}Na_{0.1}K_{0.9}Ba_{0.1}Fe_4As_4$ $T_c = 34$ K		
	Θ_E(K)	κ(eV Å^{-2})	σ_0^2(Å^2)	Θ_E(K)	κ(eV Å^{-2})	σ_0^2(Å^2)
Fe–As	313 ± 20	5.6(4)	0.0007(3)	323 ± 27	5.9(5)	0.0007(3)
Fe–Fe	216 ± 15	2.3(2)	0.0019(5)	218±10	2.4(1)	0.0016(4)

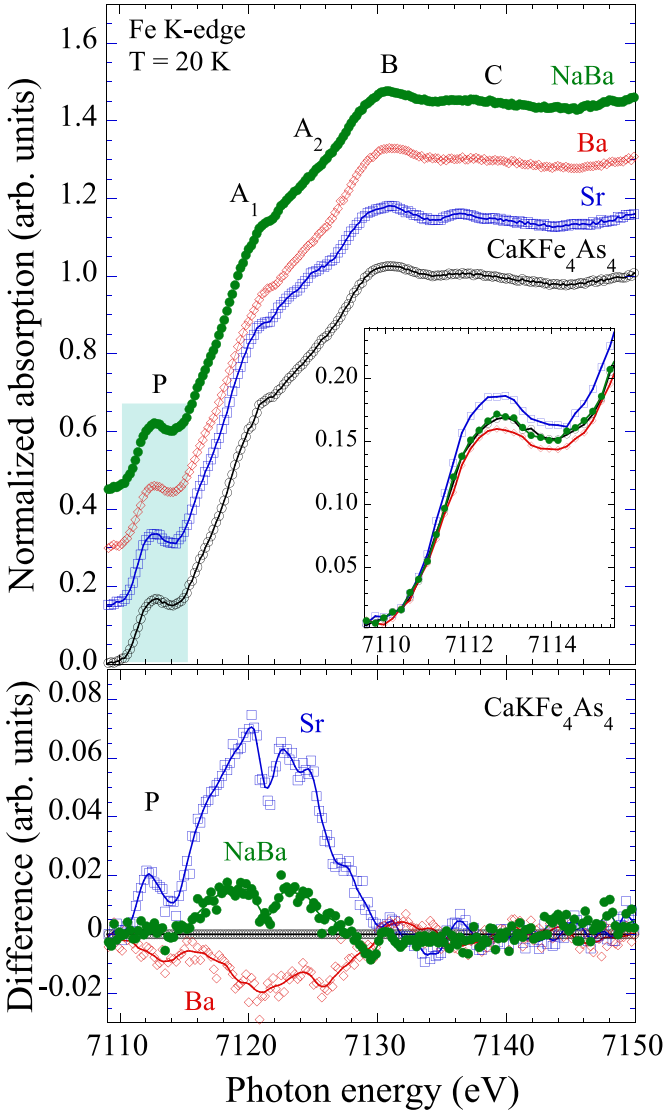

Figure 8. Normalized XANES spectra of $CaKFe_4As_4$ (black), $CaK_{0.9}Sr_{0.1}Fe_4As_4$ (blue, denoted as Sr), $CaK_{0.9}Ba_{0.1}Fe_4As_4$ (red, denoted as Ba), and $Ca_{0.9}Na_{0.1}K_{0.9}Ba_{0.1}Fe_4As_4$ (green, denoted as NaBa). The spectra are artificially shifted just for the visualization. The inset shows a zoom over the peak P. The lower panel displays the XANES differences with respect to the pristine $CaKFe_4As_4$.

the other hand, the size difference should be directly affecting the local structure. Here, it is worth recalling that the 1144 system is stable for smaller Δa and larger Δc with a and c being the average lattice parameters for the 122 substructures in the 1144 system [11, 19, 20]. At the local scale, the Fe–Fe distance for the Sr substituted $CaK_{0.9}Sr_{0.1}Fe_4As_4$ differs substantially from the one in the pristine $CaKFe_4As_4$ with the anion height being much lower. This suggests that Sr substituted $CaK_{0.9}Sr_{0.1}Fe_4As_4$ may be less stable due to the larger size difference between K and Sr Thus, it is likely that the Sr substituted system is characterized by a local texturing and filamentary superconductivity. This will be consistent with the stiffer Fe–As bonds in the Sr substituted $CaK_{0.9}Sr_{0.1}Fe_4As_4$. On the other hand, having K and Ba being almost of similar size, Ba substituted $CaK_{0.9}Ba_{0.1}Fe_4As_4$, in which bond characteristics are very similar to the one of the pristine sample, is likely to be more stable than the Sr substituted sample. Although small, the σ^2 of $CaKFe_4As_4$, $CaK_{0.9}Ba_{0.1}Fe_4As_4$, and $Ca_{0.9}Na_{0.1}K_{0.9}Ba_{0.1}Fe_4As_4$ samples tends to decrease below $T \sim 50$ K. Such a tendency is not seen in $CaK_{0.9}Sr_{0.1}Fe_4As_4$ sample, likely to be due to possible filamentary superconductivity. Incidentally, the configurational disorder suffers limited effect by small substitutions as evident from similar values of σ_0^2 for the two bonds in different samples (see table 1).

4. Summary

In summary, we have analyzed the local structure of $CaKFe_4As_4$ superconductors with different aliovalent substitution of the Ca and K sites, namely $CaKFe_4As_4$, $CaK_{0.9}Sr_{0.1}Fe_4As_4$, $CaK_{0.9}Ba_{0.1}Fe_4As_4$, and $Ca_{0.9}Na_{0.1}K_{0.9}Ba_{0.1}Fe_4As_4$, as a function of temperature. Our primary emphasis has been on the Fe–As network within this hybrid system, as the local structure of this network plays a crucial role in the electronic transport properties of these materials. For the purpose, we have exploited Fe K-edge EXAFS to determine the local near neighbor bondlengths (Fe–As and Fe–Fe) and their stiffness. The EXAFS analyses reveal that, while the Fe–As bondlength is hardly affected by the substitutions, its stiffness differs in the differently substituted samples. The Fe–Fe bondlength suffers substantial change thereby the As anion height above the Fe plane (h_z), an empirical parameter often used to describe the local structure versus the T_c in the FeSC. We have found that the Fe–Fe bond stiffness is only marginally affected by the aliovalent substitution. However, it is worth noticing that the bond stiffness is affected when the size difference between the Alkaline earth and the Alkaline metal is large. This indicates that the strain effect due to size difference should have larger effect on the local structure and the stability of the 1144 structure. It is interesting to observe that the anion height manifests a peculiar temperature dependence, similar for all the samples, with an apparent anomaly below ~100 K, possibly due to half collapsed tetragonal phase transition involving As–As axial bonding [27, 28]. Such a change in As–As bonding is expected to affect [27] the fluctuating hedgehog spin vortex states [55] below this temperature. This observation further underlines magnetoelastic sensitivity of these materials.

Data availability statement

The data cannot be made publicly available upon publication because they are not available in a format that is sufficiently accessible or reusable by other researchers. The data that support the findings of this study are available upon reasonable request from the authors.

Acknowledgments

We thank the ALBA staff for the assistance during the measurements. One of us (A D) would like to acknowledge EUROfusion. The work is partially supported by the Sapienza University of Rome and under the National Recovery and Resilience Plan (NRRP), Mission 4 Component 2 Investment 1.3 of the Italian Ministry of University and Research (MUR); funded by the European Union—NextGenerationEU—Award Number: Project code PE0000021, Concession Decree No. 1561 of 11.10.2022 adopted by the MUR, CUP B53C22004070006 Project title 'Network 4 Energy Sustainable Transition—NEST.

ORCID iDs

G Tomassucci https://orcid.org/0000-0002-2441-3796
A Masi https://orcid.org/0000-0002-1976-0603
L Simonelli https://orcid.org/0000-0001-5331-0633
V Martin-Diaconesu https://orcid.org/0000-0002-7575-2237
L Boeri https://orcid.org/0000-0003-1186-2207
T Mizokawa https://orcid.org/0000-0002-7682-2348
N L Saini https://orcid.org/0000-0003-3684-1517

References

[1] Kamihara Y, Watanabe T, Hirano M and Hosono H 2008 Iron-based layered superconductor $LaO_{1-x}F_xFeAs$ (x = 0.05 − 0.12) with T_c = 26 K *J. Am. Chem. Soc.* **130** 3296–7
[2] Hosono H and Kuroki K 2015 Iron-based superconductors: current status of materials and pairing mechanism *Physica* C **514** 399–422
[3] Fernandes R M, Coldea A I, Ding H, Fisher I R, Hirschfeld P J and Kotliar G 2022 Iron pnictides and chalcogenides: a new paradigm for superconductivity *Nature* **601** 35–44
[4] Hosono H, Yamamoto A, Hiramatsu H and Ma Y 2018 Recent advances in iron-based superconductors toward applications *Mater. Today* **21** 278–302
[5] Biswal G and Mohanta K L 2021 A recent review on iron-based superconductor *Mater. Today: Proc.* **35** 207–15
[6] Gati E, Xiang L, Bud'ko S L and Canfield P C 2020 Hydrostatic and uniaxial pressure tuning of iron-based superconductors: insights into superconductivity, magnetism, nematicity and collapsed tetragonal transitions *Ann. Phys., Lpz.* **532** 2000248

[7] Kreisel A, Hirschfeld P J and Andersen B M 2020 On the remarkable superconductivity of FeSe and its close cousins *Symmetry* **12** 1402

[8] Stewart G R 2011 Superconductivity in iron compounds *Rev. Mod. Phys.* **83** 1589

[9] Paglione J and Greene R L 2010 High-temperature superconductivity in iron-based materials *Nat. Phys.* **6** 645–58

[10] Rotter M, Tegel M and Johrendt D 2008 Superconductivity at 38 K in the iron arsenide $(Ba_{1-x}K_x)Fe_2As_2$ *Phys. Rev. Lett.* **101** 107006

[11] Iyo A, Kawashima K, Kinjo T, Nishio T, Ishida S, Fujihisa H, Gotoh Y, Kihou K, Eisaki H and Yoshida Y 2016 New-structure-type Fe-based superconductors: $CaAFe_4As_4$ (A = K, Rb, Cs) and $SrAFe_4As_4$ (A = Rb, Cs) *J. Am. Chem. Soc.* **138** 3410–5

[12] Zhi-An R, Wei L, Jie Y, Wei Y, Xiao-Li S, Zheng-Cai C G-C, Xiao-Li D, Li-Ling S, Fang Z and Zhong-Xian Z 2008 Superconductivity at 55 K in Iron-Based F-Doped Layered Quaternary Compound Sm[O1-xFx]FeAs *Chin. Phys. Lett.* **25** 2215

[13] Hanna T, Muraba Y, Matsuishi S, Igawa N, Kodama K, Shamoto S-ichi and Hosono H 2011 Hydrogen in layered iron arsenides: indirect electron doping to induce superconductivity *Phys. Rev.* B **84** 024521

[14] Tapp J H, Tang Z, Lv B, Sasmal K, Lorenz B, Chu P C and Guloy A M 2008 LiFeAs: an intrinsic FeAs-based superconductor with T_c = 18 K *Phys. Rev.* B **78** 060505

[15] Jiang X *et al* 2023 Interplay between superconductivity and the strange-metal state in FeSe *Nat. Phys.* **19** 365–71

[16] Singh S J, Cassidy S J, Bristow M, Blundell S J, Clarke S J and Coldea A I 2019 Optimization of superconducting properties of the stoichiometric $CaKFe_4As_4$ *Supercond. Sci. Technol.* **33** 025003

[17] Momma K and Izumi F 2011 VESTA 3 for three-dimensional visualization of crystal, volumetric and morphology data *J. Appl. Crystallogr.* **44** 1272–6

[18] Kawashima K, Ishida S, Fujihisa H, Gotoh Y, Kihou K, Yoshida Y, Eisaki H, Ogino H and Iyo A 2018 Superconductivity in a new 1144-type family of (La, Na)AFe_4As_4 (A = Rb or Cs) *J. Phys. Chem. Lett.* **9** 868–73

[19] Song B Q, Nguyen M C, Wang C Z and Ho K M 2018 Stability of the 1144 phase in iron pnictides *Phys. Rev.* B **97** 094105

[20] Song B Q, Nguyen M C, Wang C Z, Canfield P C and Ho K M 2018 Is it possible to stabilize the 1144-phase pnictides with tri-valence cations? *Phys. Rev. Mater.* **2** 104802

[21] Hikami S, Ishida S, Iyo A, Eisaki H, Arita M, Kumar S, Schwier E F, Shimada K, Saini N L and Mizokawa T 2022 Fermi surface geometry of heavily hole doped CaKFe4As4 revealed by angle-resolved photoemission spectroscopy *J. Phys. Soc. Japan* **91** 124704

[22] Meier W R *et al* 2016 Anisotropic thermodynamic and transport properties of single-crystalline $CaKFe_4As_4$ *Phys. Rev.* B **94** 064501

[23] Mou D *et al* 2016 Enhancement of the superconducting gap by nesting in $CaKFe_4As_4$: a new high temperature superconductor *Phys. Rev. Lett.* **117** 277001

[24] Cui J *et al* 2017 Magnetic fluctuations and superconducting properties of $CaKFe_4As_4$ studied by As^{75} NMR *Phys. Rev.* B **96** 104512

[25] Stillwell R L, Wang X, Wang L, Campbell D J, Paglione J, Weir S T, Vohra Y K and Jeffries J R 2019 Observation of two collapsed phases in $CaRbFe_4As_4$ *Phys. Rev.* B **100** 045152

[26] Huang Y-N, Yu X-L, Liu D-Y and Han M-M 2023 Role of doping effect and chemical pressure effect introduced by Alkali metal substitution on 1144 iron-based superconductors *Materials* **16** 3343

[27] Borisov V, Canfield P C and Valenti R 2018 Trends in pressure-induced layer-selective half-collapsed tetragonal phases in the iron-based superconductor family $AeAFe_4As_4$ *Phys. Rev.* B **98** 064104

[28] Kaluarachchi U S *et al* 2017 Pressure-induced half-collapsed-tetragonal phase in $CaKFe_4As_4$ *Phys. Rev.* B **96** 140501

[29] Liu W *et al* 2020 A new Majorana platform in an Fe-As bilayer superconductor *Nat. Commun.* **11** 5688

[30] Ishida S *et al* 2019 Unique defect structure and advantageous vortex pinning properties in superconducting $CaKFe_4As_4$ *npj Quantum Mater.* **4** 27

[31] Ichinose A, Pyon S, Tamegai T and Ishida S 2021 Elucidating the origin of planar defects that enhance critical current density in $CaKFe_4As_4$ single crystals *Supercond. Sci. Technol.* **34** 034003

[32] Singh S J, Bristow M, Meier W R, Taylor P, Blundell S J, Canfield P C and Coldea A I 2018 Ultrahigh critical current densities, the vortex phase diagram and the effect of granularity of the stoichiometric high-T c superconductor $CaKFe_4As_4$ *Phys. Rev. Mater.* **2** 074802

[33] Augieri A *et al* 2023 The effect of Aliovalent substitution on magnetic properties of polycrystalline Ca/K-1144 *IEEE Trans. Appl. Supercond.* **33** 1–5

[34] Masi A *et al* 2023 Aliovalent substitution in 1144 iron based superconductors: effect on structure and superconducting properties *IEEE Trans. Appl. Supercond.* **32** 7300105

[35] Masi A, Angrisani Armenio A, Celentano G , La Barbera A, Rufoloni A, Silva E, Vannozzi A and Varsano F 2021 *J. Alloys Compd.* **869** 159202

[36] Masi A, Duchenko A, Celentano G and Varsano F 2022 Tailoring the critical temperature of Ca/K-1144 superconductors: the effect of aliovalent substitution on tetragonality *Supercond. Sci. Technol.* **35** 065015

[37] Duchenko A *et al* 2024 Relation between composition and crystalline structure in substituted CaKFe4As4 *IEEE Trans. Appl. Supercond.* **34** 7300105

[38] Haberkorn N, Xu M, Meier W R, Schmidt J, Bud'ko S L and Canfield P C 2019 Effect of Ni doping on vortex pinning in $CaK(Fe_{1-x}Ni_x)_4As_4$ single crystals *Phys. Rev.* B **100** 064524

[39] Xu M, Schmidt J, Tanatar M A, Prozorov R, Bud'ko S L and Canfield P C 2023 Superconductivity and magnetic and transport properties of single-crystalline $CaK(Fe_{1-x}Cr_x)_4As_4$ *Phys. Rev.* B **107** 134511

[40] Koningsberger D C and Prins R 1987 *x-ray Absorption: Principles, Applications, Techniques of Exafs* (SEXAFS and XANES, Wiley)

[41] Bunker G 2010 *Introduction to Xafs: a Practical Guide to x-ray Absorption Fine Structure Spectroscopy.* (Cambridge University Press)

[42] Simonelli L, Marini C, Olszewski W, Avila Perez M, Ramanan N, Guilera G, Cuartero V and Klementiev K 2016 CLAESS: the hard x-ray absorption beamline of the ALBA CELLS synchrotron *Cog. Phys.* **3** 1231987

[43] Gurman S J 1995 Interpretation of EXAFS data *J. Synchrotron Radiat.* **2** 56–63

[44] Ressler T 1998 WinXAS: a program for x-ray absorption spectroscopy data analysis under MS-Windows *J. Synchrotron Radiat.* **5** 118–22

[45] Ankudinov A L, Ravel B, Rehr J J and Conradson S D 1998 Real-space multiple-scattering calculation and interpretation of x-ray-absorption near-edge structure *Phys. Rev.* B **58** 7565

[46] Joyner R W, Martin K J and Meehan P 1987 *J. Phys. C: Solid State Phys.* **20** 4005

[47] Stramaglia F *et al* 2021 Temperature dependence of the local structure and iron magnetic moment in the self-doped $CaKFe_4As_4$ iron-based superconductor *J. Phys. Chem.* C **125** 10810–6
[48] Mizuguchi Y, Hara Y, Deguchi K, Tsuda S, Yamaguchi Y, Takeda K, Kotegawa H, Tou H and Takano Y 2010 Anion height dependence of Tc for the Fe-based superconductor *Supercond. Sci. Technol.* **23** 054013
[49] Rehr J J and Albers R C 2000 Theoretical approaches to x-ray absorption fine structure *Rev. Mod. Phys.* **72** 621
[50] De Groot F, Vanko G and Glatzel P 2009 The 1s x-ray absorption pre-edge structures in transition metal oxides *J. Condens. Matter Phys.* **21** 104207
[51] Joseph B, Iadecola A, Simonelli L, Mizuguchi Y Takano Y, Mizokawa T and Saini N 2010 A study of the electronic structure of $FeSe_{1-x}Te_x$ chalcogenides by Fe and Se K-edge x-ray absorption near edge structure measurements *J. Condens. Matter Phys.* **22** 485702
[52] García Saravia Ortíz de Montellano A, Mustre de Leon J, Saini N L and Bianconi A 2012 Effect of rare earth substitution in the density of electronic states of LnOFeAs *J. Appl. Phys.* **111** 112631
[53] Hacisalihoglu M Y, Simonelli L, Marini C, Provino A, Martinelli A, Manfrinetti P, Putti M and Saini N L 2020 Mn substitution effect on the local structure of $La(Fe_{1-x}Mn_x)AsO$ studied by temperature dependent x-ray absorption measurements *J. Phys.: Condens. Matter* **33** 095803
[54] Pugliese G M, Simonelli L, Tortora L, Tomassucci G, Iyo A, Eisaki H, Mizokawa T and Saini N L 2022 Determination of the local structure of the $La_{0.5-x}Na_{0.5+x}Fe_2As_2$ superconductor *Phys. Rev.* B **105** 024519
[55] Ding Q-P, Meier W R, Böhmer A E, Bud'ko S L, Canfield P C and Furukawa Y 2017 NMR study of the new magnetic superconductor $CaK(Fe_{0.951}Ni_{0.049})_4As_4$: microscopic coexistence of the hedgehog spin-vortex crystal and superconductivity *Phys. Rev.* B **96** 220510